

# Linear Actuator Powered Flapping Wing

by

Christopher L. Benson

Submitted to the Department of Mechanical Engineering  
In Partial Fulfillment of the Requirements of the Degree of

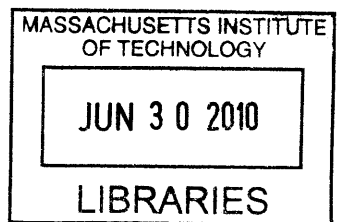
Bachelor of Science in Mechanical Engineering  
at the  
Massachusetts Institute of Technology

June 2010

©2010 Christopher L. Benson. All rights reserved.

The author hereby grants to MIT permission to reproduce  
and to distribute publicly paper and electronic copies  
of this thesis document in whole or in part in any medium  
now known or hereafter created.

**ARCHIVES**



Signature of Author \_\_\_\_\_  
Department of Mechanical Engineering  
May 10, 2010

Certified by \_\_\_\_\_  
Ian W. Hunter  
Hatsopoulos Professor of Mechanical Engineering  
Thesis Supervisor

Accepted by \_\_\_\_\_  
John H. Lienhard V  
Collins Professor of Mechanical Engineering  
Chairman, Undergraduate Thesis Committee

# Linear Actuator Powered Flapping Wing

by

Christopher L. Benson

Submitted to the Department of Mechanical Engineering  
on May 10, 2010 in Partial Fulfillment of the  
Requirements for the Degree of Bachelor of Science in  
Mechanical Engineering

## ABSTRACT

Small scale unmanned aerial vehicles (UAVs) have proven themselves to be useful, but often too noisy for certain operations due to their rotary motors. This project examined the feasibility of using an almost silent linear actuator to power a flapping wing UAV. In order to this, a wing was designed and installed into a test set-up to replicate normal flight conditions of flapping wing flight (FWF). The designs of the wing, the test set-up and the actual experiments were biomimetic, looking to approximate the flight of real birds. The main goal of this study was to characterize a novel new linear actuator being developed in the Bio-Instrumentation Lab at MIT based on important parameters for FWF including the mounting position, the frequency of oscillation and the amplitude of oscillation of the wing. Ultimately the linear actuator performed well under all of the tests and was only limited by the control software. When the frequency and amplitude of oscillation were raised, the force on the actuator increased. The mounting position ended up not having a correlation with the force on the actuator, leading one to believe that it is not a critical parameter for this actuator-wing system.

Thesis Supervisor: Ian W. Hunter

Title: Hatsopoulos Professor of Mechanical Engineering

## **Acknowledgements**

First I would like to thank Professor Hunter for providing me with the wonderful opportunity to work in the Bioinstrumentation Laboratory.

I am also greatly indebted to Bryan Ruddy, who provided a tremendous amount of guidance and support in my work. The lab as a whole has also been very helpful with their advice.

I must also thank my friends in Baker 6<sup>th</sup> for allowing me a place to stay during all the late nights of working on this, as well as the Brothers of Phi Delta Theta, who have provided me with countless hours of discussion and relaxation.

Finally I would like to thank my parents Tricia and Gary, my sister Kacey, and my grandparents Tom and Kay for always supporting me throughout my education.

# Table of Contents

Acknowledgements.....	3
Table of Contents.....	4
List of Figures.....	5
1. Introduction and Motivation Behind Research.....	6
1.1 Linear Actuators and Ornithopters.....	7
1.2 Overview of Project.....	7
2. Background.....	9
2.1 Wing Design.....	9
2.2 Flapping Wing Flight.....	14
2.3 FWF and Mini-UAVs.....	20
3. Fabrication of the Wing and the Test Apparatus.....	24
3.1 Design of the Wing.....	24
3.2 Lorentz Force Linear Actuator.....	26
3.3 Test Stand.....	27
3.4 System Electronics and Sensors.....	31
3.5 Driving Software and PID Control.....	36
4. Results and Discussion.....	48
4.1 Testing the Wing.....	48
4.2 Results and Significance.....	50
5. Conclusions and Future Work.....	56
References.....	58

## List of Figures

Figure 1: Wing design with wrist joints and flapping motion .....	11
Figure 2: Wing with MFC actuation .....	12
Figure 3: Flapping motion of MFC actuated wing .....	12
Figure 4: Wing fabrication process using photolithography .....	14
Figure 5: Wind tunnel test of smart flapping wing .....	14
Figure 6: Change in angle of attack through wing stroke .....	15
Figure 7: Comparison of optimal and sinusoidal wing flapping motion .....	16
Figure 8: Fluid force and vorticity field of optimized wing motion .....	16
Figure 9: Aerodynamic forces and wing angle compared with air speed .....	17
Figure 10: Wing beat rate of birds compared with wing length .....	18
Figure 11: Flapping frequency compared with air speed .....	19
Figure 12: Sweep angle compared with air speed .....	19
Figure 13: Change in wing flapping motion compared with air speed .....	20
Figure 14: Comparison of aerodynamic forces of an ornithopter and a bird .....	21
Figure 15: Force diagram of angle adjusted ornithopter .....	22
Figure 16: FWF wing beating mechanism .....	22
Figure 17: Fully constructed wing .....	25
Figure 18: Linear actuator installed in needleless injection apparatus and AUV .....	26
Figure 19: Solid model of linear actuator .....	27
Figure 20: Final constructed version of test stand .....	28
Figure 21: Solid Model of actuator connector .....	30
Figure 22: Final constructed version of pivoting stand .....	30
Figure 23: Solid model of wing connector .....	31
Figure 24: Block diagram of Labview virtual instrument .....	39
Figure 25: Block diagram of input section of Labview vi .....	39
Figure 26: Block diagram of output section of Labview vi .....	41
Figure 27: PID control scheme .....	42
Figure 28: Block diagram of PID section of Labview vi .....	44
Figure 29: Block diagram of signal simulator section of Labview vi .....	45
Figure 30: Block diagram of file writing section of Labview vi .....	47
Figure 31: Comparison of mounting positions for wing pivot .....	49
Figure 32: Calibration curve for position sensor .....	51
Figure 33: Calibration curve for force sensor .....	52
Figure 34: Effect of sweep amplitude on actuator performance .....	53
Figure 35: Effect of oscillation frequency on actuator performance .....	53
Figure 36: Desired and actual position of actuator at 5 Hz .....	54
Figure 37: Effect of pivot mount point on actuator performance .....	55
Figure 38: Test set-up including horizontal and vertical force sensors .....	56

# 1. Introduction

For centuries humans have been interested in the notion of flying, countless inventors have tried to create flying machines dating back thousands of years. More recently, people have begun to look to nature to inspire their attempts at flight. Many people have studied the flight of birds and the design of their wings in an attempt to replicate what nature has done so well in the hopes that a new flying machine can be made in that image.

More recently, small form unmanned aerial vehicles (UAVs) have been proven to be effective on the modern battlefield and in other areas for real time aerial surveillance. These vehicles are often carried by a single person, weigh less than ten pounds, have a wingspan of approximately four feet and are usually mounted with either visual or infrared cameras<sup>12</sup>. They have shown the ability to collect massive amounts of real time visual data, helping many military operations and search and rescue missions. One of the main downsides of these vehicles is their high noise output, which can be counterproductive to surveillance missions.

The source of the noise that UAV produce is almost always contributed to the loud rotary power source, whether it is a propeller or a small jet engine. There have been several attempts to address the noise issue to little avail. The most effective strategy to collect significant amounts of data without being detected has been to use “parasite” UAVs, which are released from another vehicle such as a cruise missile or a large UAV and are unpowered, but can have glide times of up to ½ hour<sup>12</sup>. This situation leaves room for improvement in glide time, vehicle launch, and vehicle recovery. Human portable

UAVs are effective because they can be launched at will without significant extra equipment and can easily be landed back where they were launched without the need for additional danger when recovering the vehicle.

One option for making the small UAVs operate more quietly is to use a powerful yet light, linear actuator to power flapping wings. This would eliminate the loud aspects of the rotary power source and allow for easy launch, recovery and elongated flight times through powered flight.

## **1.1 *Linear Actuators and Ornithopters***

Ornithopters are essentially flapping wing flying machines that fly using similar motions as birds. They have many benefits over more traditional forms of flight, but are rather difficult to build and often are plagued by reliability issues. One method that has not been tested extensively before is using a linear actuator to power an ornithopter. This research looks to give a first order approximation to answer if an actuator is potentially feasible for use in ornithopters in order to decide if more research should be done on using linear actuators for this new application.

## **1.2 *Overview of Project***

The goal of the project is to provide a physical testing apparatus for the new linear actuator developed in the bioinstrumentation lab at MIT. This will allow the actuator to be tested and characterized in a physical situation.

The first step in completing this research was to study the characteristics of wings and the motion of flight. Wings have many unique characteristics that make them suitable

for flying, therefore these properties must be understood before creating a realistic test wing for the actuator to be attached to. In particular, the structural support and material choice of the wing were critical, as the wing was designed to be an approximation of a real bird wing. The wing was be designed to be light weight and structurally sound, and was kept rigid in this experiment for the sake of ease of manufacturing, even though most wings deform through normal flight.

In order to operate the wing, a structure was built to attach the actuator to the wing and allow for motion so that the wing could flap. This structure was designed and built to be very robust, as the power input into the actuator can be rather large and thus a flimsy structure could have broken under the testing loads. Once the test stand was built to house the actuator and connect it to the wing, sensors were installed throughout the entire system. These sensors measure the position of the wing-actuator set-up, the output voltage being sent to the wing, and the amount of force that the actuator produces. Once the sensors were hooked up, a program was written to control the system and record the measurements being taken by the varying sensors.

After everything had been combined together and the kinks worked out, the wing-actuator system was tested against three variables: the mounting position of the wing pivot point along with the amplitude and frequency of the oscillation of the wing. In the end, the wing was tested under 90 different sets of conditions and the data analyzed to determine the performance characteristics of the wing-actuator system.

## **2. Background**

In order to better understand how to design the experimental set-up and the important parameters to test, a better understanding of current practice of wing design and flapping wing flight was needed.

### **2.1 *Wing Design***

One of most critical aspects of a flying machine or system is the design of the wing. The wing is the part of the system that actually produces lift and feels most of the aerodynamic forces that are present on the system. Specifically the design of a wing must take into account the following factors:

- Wing Area
- Aspect Ratio
- Flexibility/multiple joints
- Material Selection
- Manufacturing Process

Most often in wing design, especially for ornithopters and vehicles designed for flapping wing flight (FWF), the initial approach is biomimetic. A biomimetic approach is one where the design of a system, in this case a wing, is based upon the structures and functions of those found in nature. Essentially what this means is that instead of starting over from scratch in designing a wing, it is possible to use current biological knowledge to create a starting point that can then be modified to suit the needs of the application.

Keeping this in mind, the area of the wing is a rather important characteristic, and can greatly affect the performance characteristics of any flying motion using the wing. The area of the wing is simply the total surface area on one side of the wing. The wing area directly corresponds to the amount of lift that a wing can produce<sup>11</sup>. Like most things in design, however, there is a balance between having too small of a wing and too large of a wing. A wing that is too small will not provide enough force to allow the system to fly or move around, while a very large wing could be potentially unwieldy and will have a larger moment of inertia which will greatly increase the power requirements from the effector<sup>8</sup>.

The actual wing area must be optimized for the particular needs of a system. For example, smaller wings provide more maneuverability, but require higher frequencies to fly. Larger wing areas are used when a system needs to glide for long periods of time<sup>10</sup>. Due to the complex nature of flight, selecting an appropriate wing area can be difficult and often requires several iterations after live testing in order to optimize it for the needs of the system.

Another morphological parameter involved in wing design is the aspect ratio. The wing aspect ratio is the ratio of the maximum length to the maximum width. The aspect ratio also affects the moment of inertia of the wing, with a larger aspect ratio resulting in a larger moment of inertia, which will require more power from the effector to operate the system<sup>7</sup>. Although there are many design parameters that are quite different for FWF wings and traditional airfoils, the cross section of a wing for both should be designed very similarly<sup>10</sup>.

Similar to those found in nature, most wings designed for FWF are somewhat flexible to allow for wing deformation throughout the flapping motion. Figure 1 shows an example of a wing that has a wrist joint at the end of the wing and corresponding computer simulations of how the wing may flex in order to accommodate FWF.

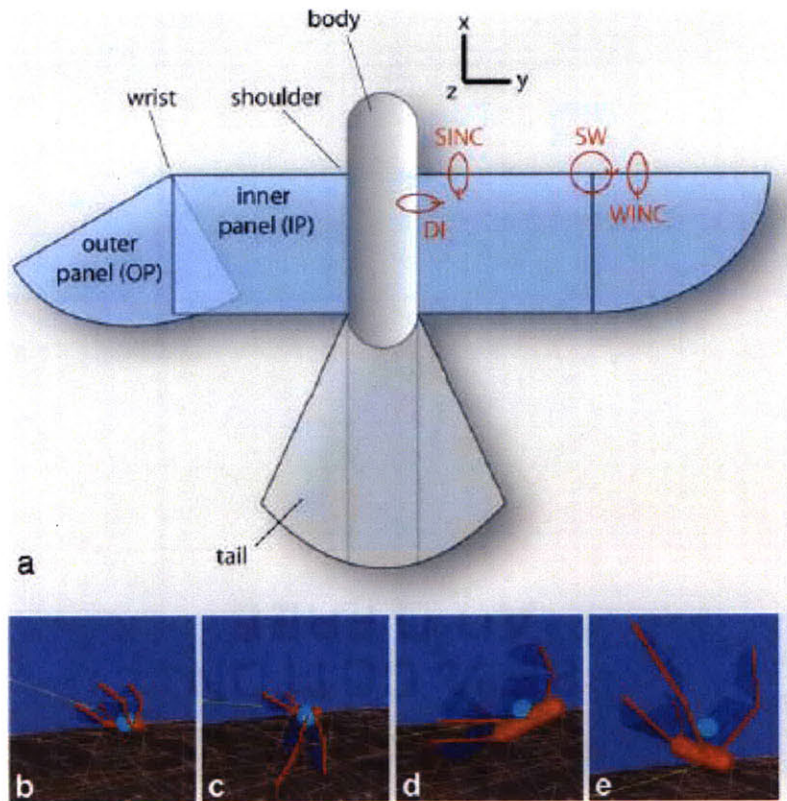


**Figure 1: Wing design with wrist joint and corresponding flapping motion.  
Taken from Margerie et al.<sup>7</sup>**

While some examples show a clear joint that can move at the end of the wing, other designs use more sophisticated technologies such as the wing design in Figure 2, which uses a Macro-Fiber Composites (MFC) actuator to allow the wing to flex mid-span. The two designs differ quite significantly in their use of a flexible wing, which also greatly affects how the wing should be oscillated to create FWF.

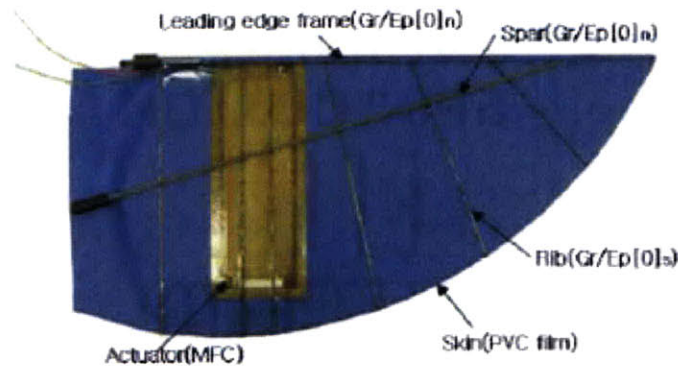


**Figure 2: Wing with MFC actuation. Taken from Kim and Han.<sup>6</sup>**

As show in Figure 3, the flapping motion of the MFC actuated wing has significantly less mid-span flex than the wing with the wrist joint.

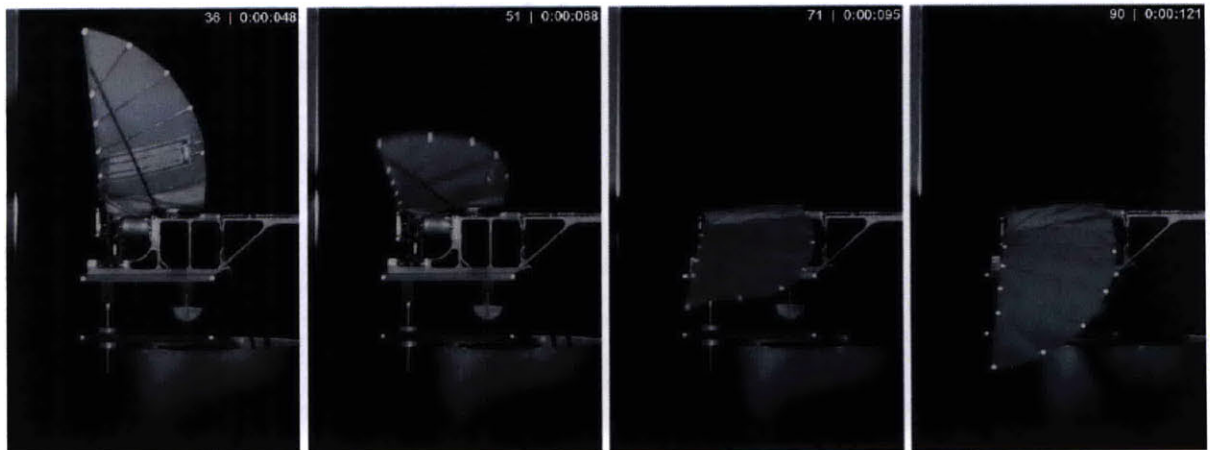


**Figure 3: Flapping motion of MFC actuated wing. Taken from Kim and Han.<sup>6</sup>**

Selecting appropriate materials is another critical aspect of designing a wing for FWF. The materials need to be strong and lightweight, but also allow for some flexibility for the mid-span joints. One of the most important considerations for material selection is its weight. As mentioned previously, any additional weight on the wings greatly increases

the power output required for FWF<sup>10</sup>. Many wings are made out of carbon fiber due to its low weight and high elastic modulus of approximately 300 GPa<sup>10</sup>. The skin of the wing must also be lightweight and strong as it will feel a considerable amount of force throughout the wing strokes.

Despite the low quantity of production, design for manufacturing is incredibly important in creating a wing for FWF because the scales and tolerances of many of the designs can be rather difficult to work with. There have been a number of advanced techniques that proved successful in creating appropriate FWF wings. Some more advanced techniques can be used for more intricate wing designs such as used by Shang et al to create fly wings as shown in Figure 4.

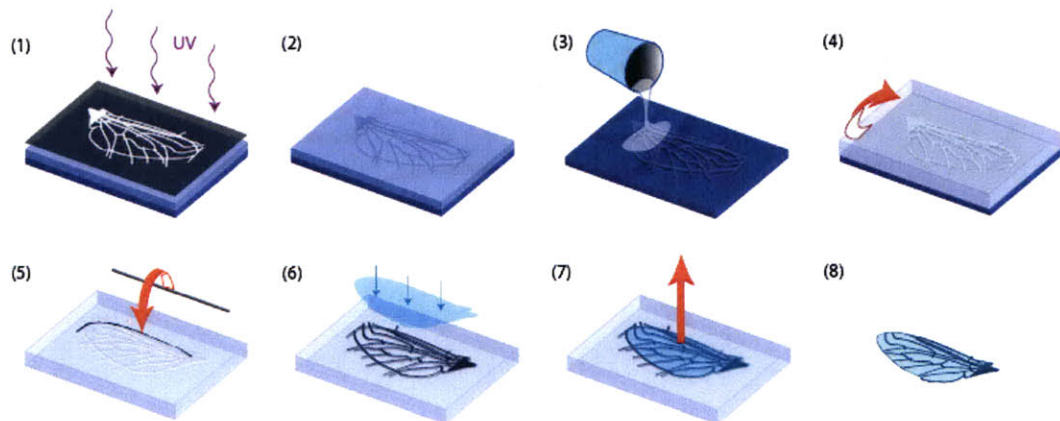


**Figure 4: Wing fabrication process using photolithography. Taken from Tobalske.<sup>11</sup>**

Kim and Han crafted their wing out of a thin PVC film and used carbon fiber rods as the frame<sup>6</sup>. The design has already been tested and proven on a micro sized system as shown in Figure 5.

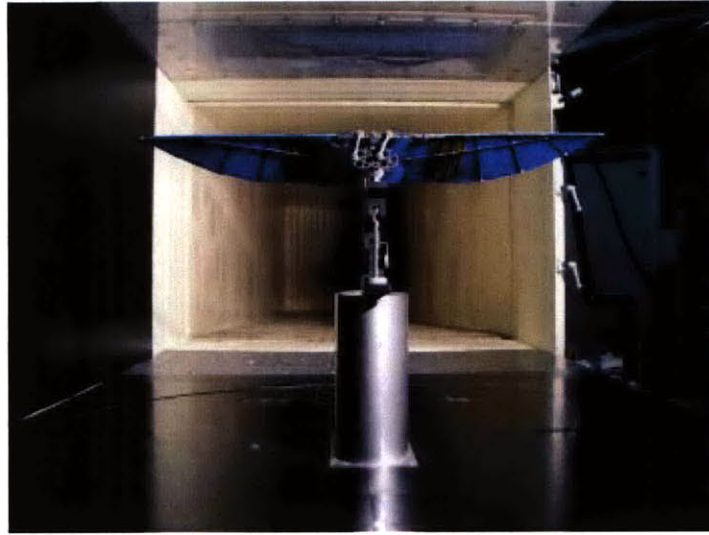


**Figure 5: Wind tunnel test section of smart flapping wing. Taken from Kim and Han.<sup>6</sup>**

## **2.2 *Flapping Wing Flight***

Most human-made flying machines use simple forward motion to generate lift, flapping wing flight (FWF) is much more complicated. There is still no complete analysis on the motion of FWF. The motion of a wing during the flapping motion is not simply up and down, but is rather up and down and forward and backwards, all combined with an ever changing angle of attack<sup>10</sup>. The motion of FWF can be broken down into several key differences from conventional flight.

- Changing Angle of Attack
- Wing beat frequencies and amplitudes
- Deviations in normal flying patterns

## 2.2.1 Angle of Attack

The angle of attack is the “angle of the plane swept out by the wing during the wing stroke”<sup>9</sup>. This aspect varies considerably from conventional flight in which the airfoil is positioned at the most efficient angle for straight and level flight at all times. With FWF the angle is constantly changing to create different effects<sup>9</sup>. The changing angle of the wing can be approximated as consistent throughout the wing stroke as shown in Figure 6.

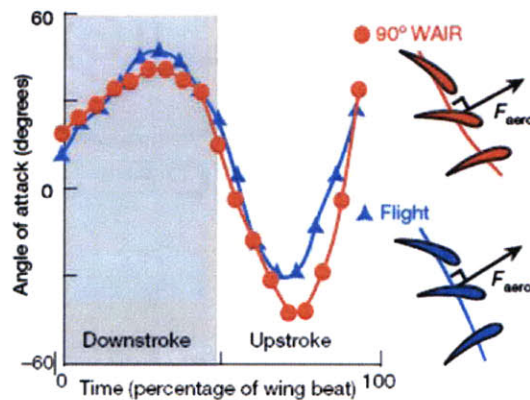


**Figure 6: Change in angle of attack through wing stroke. Taken from Poore et al.<sup>9</sup>**

Although the change in angle can be approximated by a periodic function, the optimal flapping motion uses 27% less power. Figure 7 shows a comparison between the optimal flapping motion and the sinusoidal approximation.

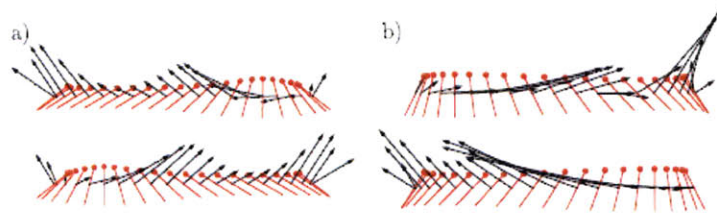


**Figure 7: Comparison of optimal and sinusoidal wing flapping motions. Taken from Pesavento et al.<sup>8</sup>**

Unlike conventional flight which can fly at the optimal angle for level flight at all times, FWF has some instances where it has to fly with a less efficient attack angle. The least efficient time during a wing stroke is during the wing reversal in between strokes when the wing switches from up to down stroke. Figure 8 shows the aerodynamic forces and vorticity for the wing throughout a wing stroke. The spikes in y-axis forces at  $\sim 3.3$  and 3.9 seconds show the stroke reversal inefficiencies<sup>8</sup>.

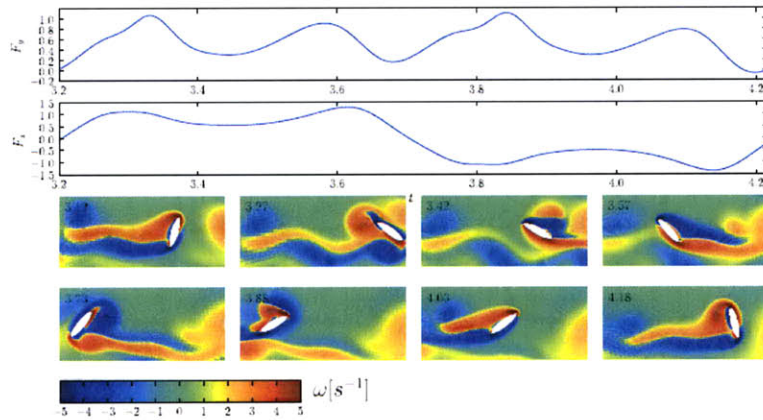


**Figure 8: Fluid force ( $F_x$  and  $F_y$ ) and vorticity field of optimal wing motion. Taken from Pesavento et al.<sup>8</sup>**

The forces on the wings and therefore the angle of attack change significantly with change in forward air speed. Figure 9 shows that as the forward air speed lessens, more extreme angles are required to handle the much larger forces than at higher speeds<sup>7</sup>.

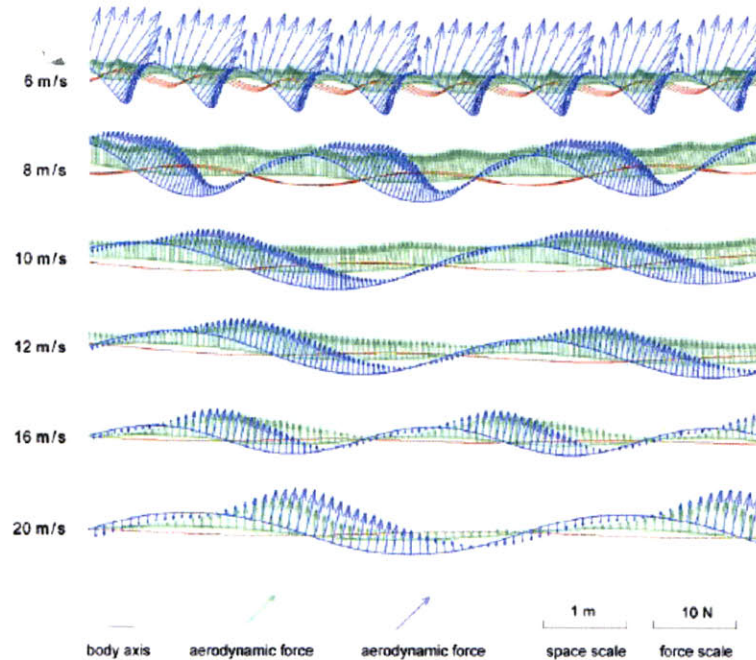


**Figure 9: Aerodynamic forces and wing angle as they vary with air speed.**  
Taken from Margerie et al.<sup>7</sup>

Although the majority of FWF can be simplified to a periodic motion, nature shows that true FWF required both periodic and non-periodic motions, which can be difficult to control

### 2.2.2 Wing beat frequencies and amplitudes

Some of the most important kinematic parameters for designing a FWF system are the flapping frequency and stroke amplitude. These parameters can greatly change the performance of a FWF system and need to be tuned based upon the characteristics of the system and the intended use of the motion.

Once again it makes the most sense to look to nature for a starting point for these parameters. Figure 10 shows the wing beat rates of many birds based upon their wing length.

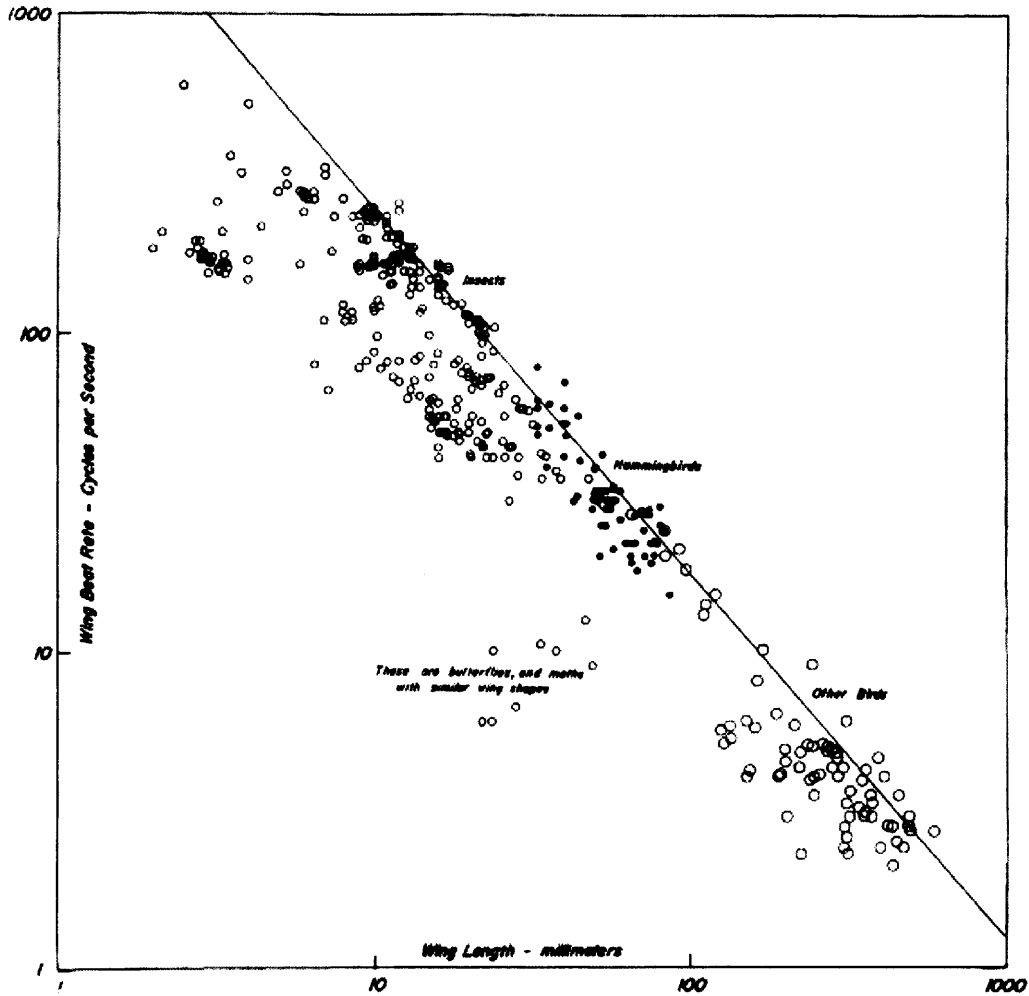
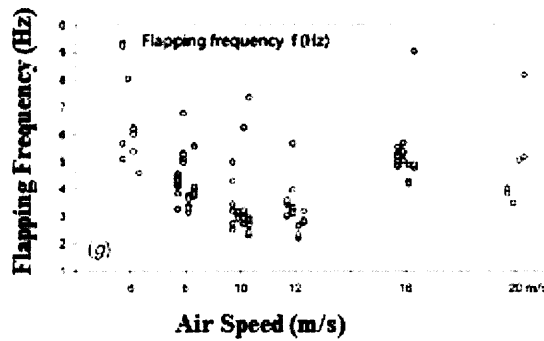


Figure 10: Wing beat rate compared with wing length for natural flyers.

Taken from Greenewalt.<sup>5</sup>

While insects and hummingbirds have very fast wing beat rates, most birds flap their wings between 3 and 10 times per second. Like the wing angle, the flapping oscillation frequency also changes with airspeed as shown in Figure 11<sup>7</sup>.



**Figure 11: Flapping frequency of birds compared with air speed. Adapted from Margerie et al.<sup>7</sup>**

The frequency is lowest at intermediate speed of 10 to 12 m/s which is where most flight takes place. As the speeds drop too low or get up to very fast the frequency increases. At intermittent speeds, the frequency of oscillation for most birds is around 3 Hz.

The stroke or sweep amplitude also changes with airspeed, resulting in much larger strokes at lower speeds. At intermittent speeds, most birds will fly with around a 20 degree sweep amplitude as shown in Figure 12.

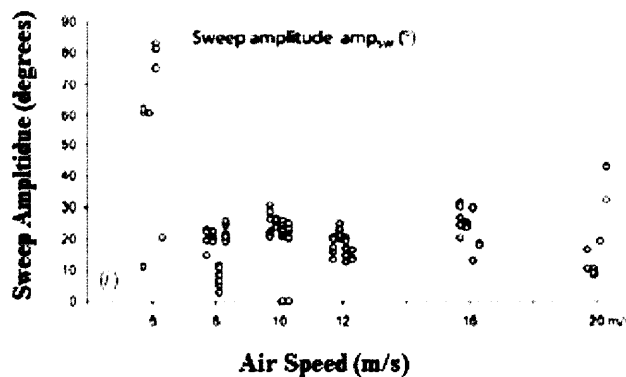


**Figure 12: Sweep amplitude of birds compared with air speed. Adapted from Margerie et al.<sup>7</sup>**

When birds use FWF they change their wing orientation from the standard motion to perform maneuvers. When this happens, it is almost always during the down stroke. The down stroke also provides most of the stability during normal level flight<sup>11</sup>. In addition to changing the flying patterns based upon maneuvers, birds will also change how they fly based upon their forward airspeed as shown in Figure 13.

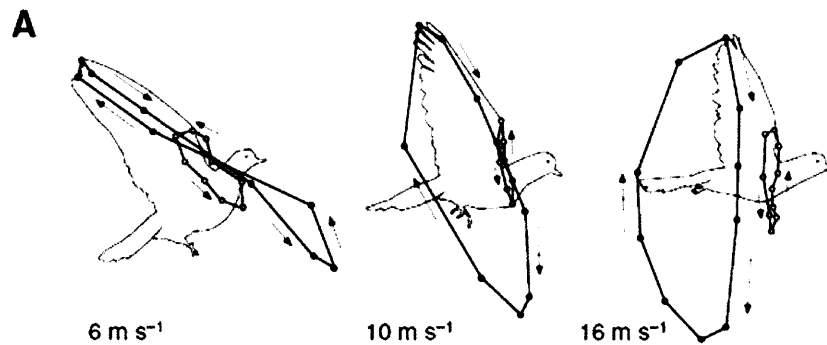


**Figure 13: Change in wing flapping motion compared with air speed. Taken from Tobalske.<sup>11</sup>**

One of the most useful parts of FWF is the fact that the wings can be used to glide and therefore sometimes the wings do not flap and the bird or vehicle can remain flying. Finding a way to create effective gliding is one of the major goals in designing FWF vehicles<sup>8</sup>.

### **2.3 FWF and Mini-UAVs**

Although FWF introduces a great many number of challenges, it has the potential to bring significant improvements to UAVs. There is a unique combination of characteristics that make the idea of a FWF UAV exciting. A UAV using FWF would have much higher maneuverability due to the unstable nature of flight. Something than many UAVs have been working towards is the ability to glide in order to greatly extend

usable range, and FWF is innately more suitable for gliding than traditional flight. FWF could allow a UAV to glide over a target at very slow speed, which would be ideal for surveillance as there would be ample time to take pictures and because the UAV would be virtually silent as it glides. Another advantage FWF brings is the increased suitability for catching air currents to extend the range even further<sup>8</sup>.

One of the biggest problems of FWF UAVs is that they currently cannot match the flight characteristics of that of natural FWF. In particular FWF vehicles produce a significant amount more thrust than birds, but produce very little lift in comparison. Figure 14 shows the comparison of aerodynamic forces between an ornithopter and a bird<sup>6</sup>.

**Table 1: Comparison of aerodynamic forces between ornithopters and birds at horizontal flapping axis.**

Stroke	Ornithopters		Birds	
	Lift	Thrust	Lift	Thrust
Down	++	++	++	++
Up	--	++	+	-
Sum		++++	+++	+

**Figure 14: Comparison of aerodynamic forces between an ornithopter and a bird. Taken from Kim and Han.<sup>6</sup>**

The result of the unbalanced forces means that often FWF vehicles have trouble creating enough lift to stay flying. One approach to solve this problem is to simply orient the entire system upwards so that some of the thrust can be converted into lift as shown in Figure 15.

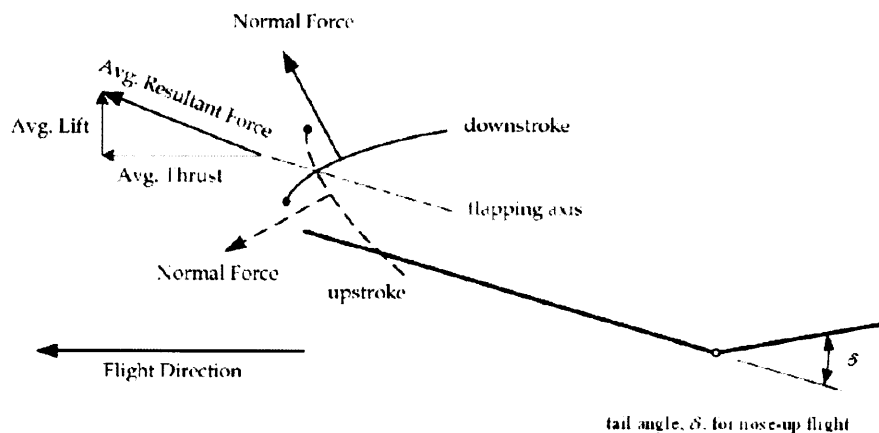


**Figure 15: Force diagram for an angle adjusted ornithopter. Taken from Kim and Han.<sup>6</sup>**

Beyond the inherent difficulties in producing a FWF UAV, there are some difficult design issues in creating a small system that can output a significant amount of power. This problem is made difficult by the need for independently flapping wings and thus requires either two effectors or a complex linkage system to allow each wing to beat at different arbitrary positions. Powering the effectors is also a very difficult problem, as the energy required to flap a wing is considerable, and conventional batteries do not provide ideal energy to weight ratios. These issues have been alleviated somewhat in recent years due to advancements in energy storage, effector power, and the miniaturization of electronics. All of these advances have resulted in some working mechanical FWF systems such as the one shown in Figure 16<sup>4</sup>.

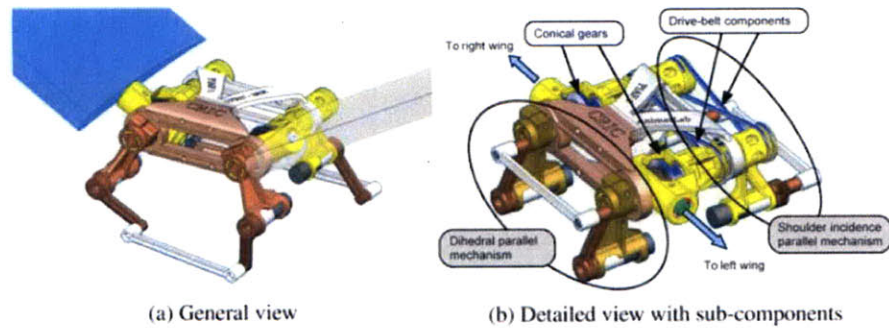


**Figure 16: FWF wing beating mechanism. Taken from Grand et al.<sup>4</sup>**

This complex mechanical system is run off of a rotary motor and consumes ~20 to 50W/kg and of power at the moderate speed of 10 to 12m/s.

There has yet to be a working FWF vehicle power by a linear actuator. The inclusion of a linear actuator as the effector could make more sense in terms of biomimetic design. Many of the designs try to imitate nature and birds, but the kind of effectors that are commonly used are not found in nature. Things like propellers and rotors are being used even though muscles are reciprocating power effectors. It is for this reason that the possibility of a linear actuator may bring a new light to the field of FWF UAVs.

### **3. Fabrication of the Wing and the Test Apparatus**

Fabrication was the most involved part of the entire experiment, much care needed to be taken in order to ensure that the subsystems were able to interact properly.

#### **3.1 Design of the Wing**

The wing is the part of the system that will attempt to replicate real forces and simulate the use of the actuator in a FWF UAV application. It is for this reason that the wing was designed to be used in a FWF vehicle. In designing the wing, there were several important aspects to consider in making it appropriate for testing the linear actuator:

- Wing Span
- Wing Area
- Material Selection

In an attempt to create a first order model, the design of the test wing was based on the synthetic wing created by Kim and Han<sup>6</sup>. The reasoning behind this is that the design was already tested and proven on a similar sized system. Using a similar design also allows the results to be compared to previous results by other groups.

Guiding off of the other design, the wing for the linear actuator system has a skeleton frame covered in a thin skin. The semi-span of the wing is 0.27m and the wing area is 0.037 m<sup>2</sup>, and the final design had an aspect ratio of 4:3. Figure 17 shows the final version of the wing.

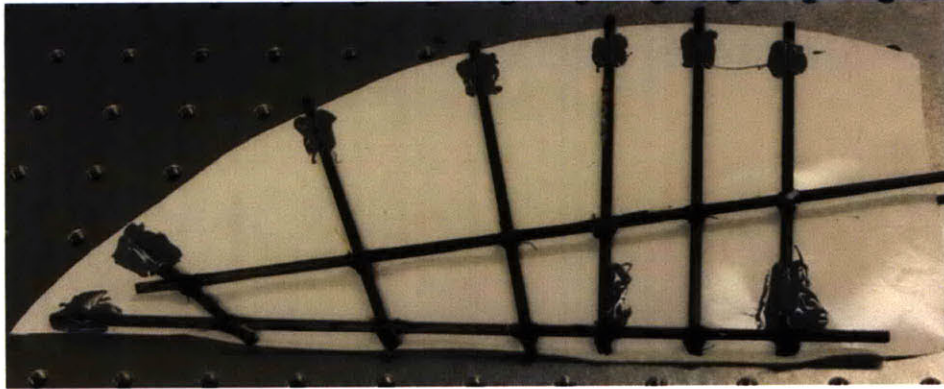


**Figure 17: Fully constructed wing.**

The skeleton structure consists of 8 cylindrical rods made out of carbon fiber. The rods are arranged based on the pattern given by Kim and Han<sup>6</sup>. The basic layout of the rods is one bar along the leading edge that is connected to 6 other supporting bars that span to the trailing edge of the wing, this gives the wing skin plenty of support to handle the forces that it incurs during the flapping motion. The supporting frame is all attached to a driving beam, which is the longest carbon fiber rod that runs diagonally across the rest of the wing. The angle of this bar is  $15^\circ$ , which comes from the layout of other ornithopter designs that have the wing slightly pointed forward to help with the changes in wing stroke in an attempt to convert more forward thrust into lift<sup>3</sup>.

The rods in the skeleton frame are connected by winding Kevlar thread around the intersections along with a thin coating of Loctite (Loctite Corporation, Rocky Hill, CT) Black Max 380 Super Glue to keep the Kevlar thread in place.

The skin of the wing is made out of a PVC film that is only  $114 \mu\text{m}$  meters thick. The PVC is a lightweight, yet durable choice for the skin. A standard two-part epoxy from Hardman (Hardman Adhesives, Milford, NH) called Double Bubble was used to connect

the wing to the frame. This epoxy is not only strong, but it is somewhat flexible, which is appropriate to connect the wing to the PVC as there was some flexing of the beams throughout the flapping motion.

### **3.2 Lorentz Force Linear Actuator**

The linear actuator used to power the system is a unique design created in the Bioinstrumentation Lab based upon a S.M Thesis by Nate Ball in 2007. The linear Lorentz force actuator was originally designed for applications in autonomous underwater vehicles (AUVs) and needle free injection. The two original use cases are shown in Figure 18.

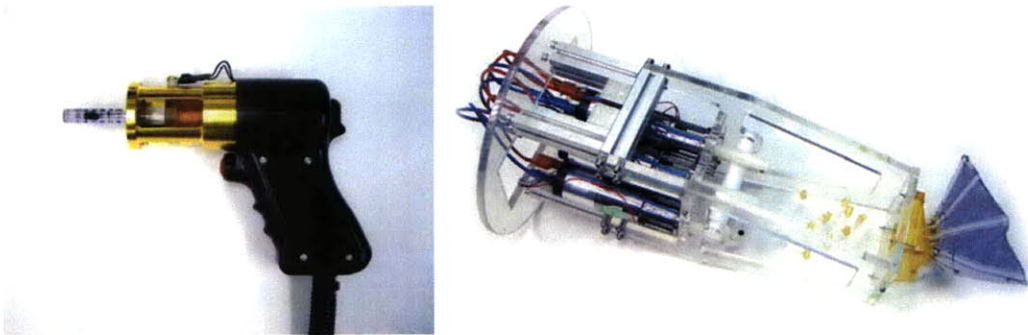


**Figure 18: Linear actuator installed in needleless injection apparatus and AUV apparatus. Taken from Ball.<sup>2</sup>**

The actuator consists of an outer shell with a permanent magnet in the center that affects the cylindrical coil that fits over the permanent magnet and also acts as the actuating part of the system. Figure 19 shows the different components of the actuator and how they fit together. The final version of the actuator used in the wing set-up used a different connector that will be explained more in depth in later sections.

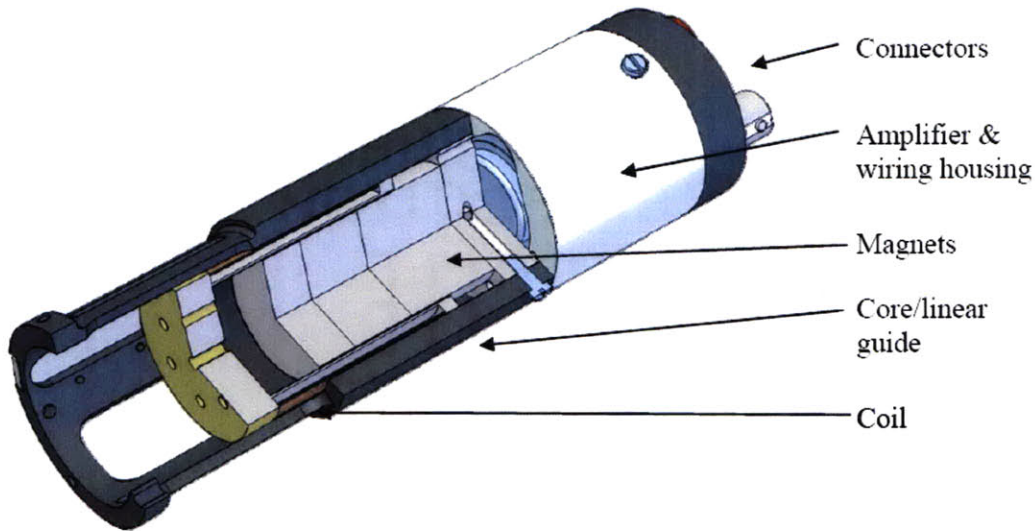


**Figure 19: Solid model of linear actuator. Taken from Ball.<sup>2</sup>**

The outer shell of the actuator is machined out a piece of steel on a 4-axis lathe. This process was very time consuming as the tolerances on the fit between the coil and the housing are very tight and the part itself is rather intricate. The coil is wrapped around a plastic core that allows for 4 layers of coiling in order to create the most power possible.

Once the coil was wound, it must be strung through the top of the coil core so that it could be connected to the power source. Connecting the power source is as simple as attaching wires to set-screws and screwing them into the corresponding pockets in the coil core. The final step is attaching the potentiometer which will be discussed in more detail in later sections.

### **3.3 Test Stand**

The test stand is the largest component of the system and is what connects all of the other pieces together. The wing and the actuator are connected through the test stand.

Several iterations of the test stand were experimented with before settling on the final design. The final constructed version of the test stand is shown in Figure 20.



**Figure 20: Final constructed version of the test stand.**

The test stand is built upon a structure of MK members (MK Technology, Bloomfield, CT) that were easily attached to the floating table which the entire experiment was built on. The test stand required three custom parts to connect the various components of the system.

- Actuator connector
- Pivoting Stand
- Wing connector

There were two methods that could have allowed the wing and actuator to interact without over-constraint: a sliding joint on the connection between the driving shaft and the

wing connector, or have the entire actuator pivot as necessary. Sliding joints are often unreliable and can cause problems, therefore the final design of the actuator connector needed to allow the actuator to pivot during motion.

The actuator connector was machined out of a brass cylinder and was designed to connect to the bottom of the actuator and to have pivoting members allow the actuator to pivot as necessary during the flapping motion. In order to machine the connector, a 4-axis lathe was used to ensure that the holes drilled into the connector would line up with those on the bottom of the actuator and that the holes for the pivoting beams were exactly  $180^\circ$  apart from each other to allow for pivoting. Figure 21 shows the solid model of the actuator connector.

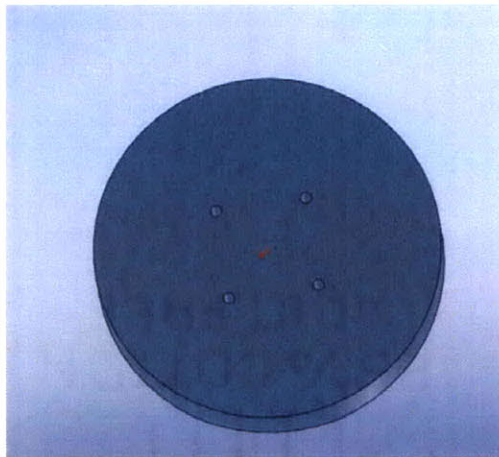


**Figure 21: Solid model of actuator connector.**

The pivoting stand is the stand that allows the actuator to pivot during the flapping wing motion. The pivoting stand has holes for the pivoting beams to go through and uses plastic rulon LR bearings to reduce friction during the pivoting motion. The entire pivoting stand is actually three pieces assembled together to allow the pivoting beams to be

fully constrained from translating. The bottom piece attaches to the MK structure, and the side pieces are attached via bolts that screw into the bottom section of the pivoting stand. Figure 22 shows an image of the pivoting stand with the shell of the actuator attached.

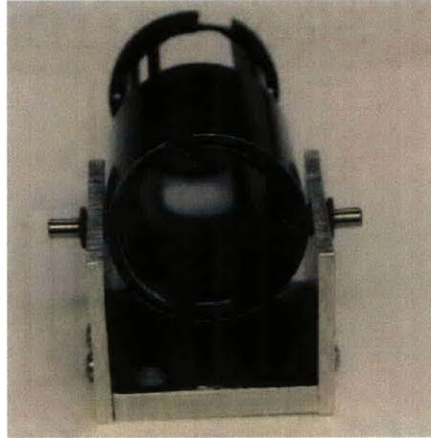


**Figure 22: Pivoting stand.**

The wing connector is the most complex piece and is used to connect the wing to the test stand and to the driving shaft of the actuator. Figure 23 shows the solid model of the connector. The connector itself was fashioned out of PVC because it is very soft and easy to machine. The wing connector has a hole for the diagonal beam of the wing to be inserted in, along with a slot for a set screw that can be used to set the attack angle of the wing. The opposite side of the connector has a hole to allow for the connector to pivot relative to the bracket mounted on the MK structure.

Finally the driving shaft of the connector is attached to the wing connector via a hole that also allows the shaft and the connector to pivot in relation to each other. In order to allow the pivoting motion, a channel was milled into the wing connector, allowing the shaft to rotate within the connector. The channel was drilled long enough to allow for an

approximately  $130^\circ$  sweep angle, which is more than enough to simulate the motions of real FWF.

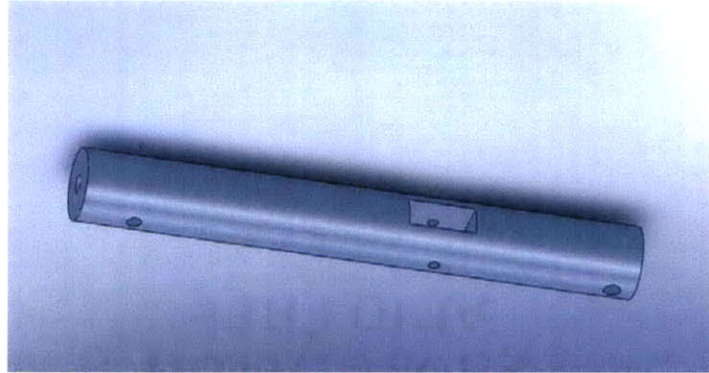


**Figure 23: Solid model of wing connector.**

### **3.4 System Electronics and Sensors**

Once the entire system was built the motor needed to be hooked up to a power source and sensors, and a controller needed to be installed in the system. All of these components were combined together to create one working system that drove the motor and the wing and measured the important system parameters. The entire system is connected through a National Instruments (National Instruments, Austin, TX) USB-6215 data acquisition system (DAQ) that is controlled by a computer running National Instrument LabView Software version 9.0.

#### **3.4.1 Power Source**

The linear actuator is powered by the analog output from the National Instruments USB 3512. The signal from the DAQ proved too weak to operate the linear actuator at high voltages and high currents. The actuator requires voltages up to 10 V (user limited) and 8 A, which proved far too high for the DAQ to handle. In order to mitigate this

problem, the output signal from the DAQ was sent through a Kepco (Kepco Inc, Flushing, NY) power amplifier that is designed to handle up to 20 V and 8 A simultaneously. This solution proved effective, as the amplified signal had no problems powering the linear actuator.

Once the power amplifier was set-up, the gain needed to be set to allow a known amount of voltage going to the actuator. The power amplifier can be run in two modes: Voltage Controlled or Current Controlled. The voltage controlled mode was appropriate for this application as it prevents the amplifier from destroying itself by attempting to output too much voltage. Ultimately the appropriate gain for the power amplifier was a factor of 5, meaning that a 1 V output from the DAQ will output 5 V to the linear actuator.

### **3.4.2 Sensors**

To measure the important parameters in the system, sensors needed to be hooked up to the linear actuator and the power amplifier. These sensors allowed the system to have a feedback loop as well as measuring relevant information about the performance of the actuator. The two important values that were measured were the position of the actuator and the force on acting on the actuator.

In order to control the position of the wing, it is important to know exactly what position the actuator is currently in. To accomplish this, a potentiometer was hooked up to the linear actuator, giving a linear range of voltages based upon the specific position the actuator was in.

The output of the potentiometer is simply a voltage, which needed to be converted to the position of the actuator by a calibration. Although the final testing will be done with

the actuator oriented vertically, it was possible to position the actuator horizontally for this calibration, as it is not a dynamic measurement and the forces of friction and gravity have no effect on the voltage output from the potentiometer. The process of calibrating the potentiometer involved simply moving the actuator to different known positions and reading off the corresponding voltage measurements from the potentiometer.

Although it sounds relatively simple, measuring the known positions of the actuator was particularly difficult, and it was very important to clearly define how the distances were measured, because even though the choice of reference point is arbitrary, the calibration would have proven useless without a consistent point to measure from. Ultimately it proved too difficult to get one consistent distance measurement on the actuator, therefore the mean of three measurements was used for the known position value and was related to the resulting voltage output of the potentiometer.

After a satisfactory number of measurements had been taken, the output voltages were plotted against the position measurements to find a correlation function that will be discussed in a later section.

One of the most relevant characteristics in measuring the performance of the actuator is the amount of force it outputs under certain circumstances. Unfortunately force can be rather difficult to measure on a continuously oscillating wing. To get around this problem, it can be assumed that the force that the actuator is outputting is related to the amount of current going into the actuator. This means that an indirect way of measuring the force is measuring the input current. The issue with measuring current was that the DAQ system being used for the measurement of the signals can only read voltage signals.

In order to solve this problem, the amount of current can be measured via the amount of voltage drop across a known resistor. This means that in order to measure the force coming out of the actuator, the voltage drop across a resistor hooked up to the input signal must be made. This resulted in few other issues that needed to be addressed, as the voltage drops across the resistor were rather small and were actually overwhelmed by the noise of the system, making the results not useful. To amplify the signal and make it more useful, a simple inverted amplifier circuit was created to boost the magnitude of the voltage.

Selection of the appropriate resistor also proved to be an important task, as the resistance needed to match up with the resolution of the DAQ system and the resistor itself needed to be able to handle a large amount of current and voltage passing through it without burning out. The appropriate size resistor was selected to use most of the range of the DAQ to allow for the most resolution possible. The range of the output was 10 V and it is a 16 bit DAQ, therefore the resolution of the DAQ controller was 0.153 V. The noise of the DAQ controller is given as 0.0012 V, which is small enough not to effect the measurements with a resolution value of 0.153 V. Using the largest expected current output, the appropriate resistor for the set-up was a 0.02  $\Omega$  resistor.

In addition to the specific resistance value of the resistor, the component needed to be extra resilient to large power loads. Ultimately a resistor from Digikey (PN 13FPR020E-ND) was selected with a resistance of 0.02  $\Omega$ , rated for 3 W and had 4 terminals to measure the force output of the actuator. The 4 terminals were selected to make the measurement of the voltage more accurate and easier to set up.

Once the voltage was measured across the resistor, it was still too small to be useful in measuring the force – as the output was simply too small for the DAQ controller to read. To address this issue, a simply inverting amplifier set-up was used to amplify the signal before sending it to the DAQ controller. Using an AMP02 amp from Analog Devices (Analog Devices, Norwood, MA) the signal was amplified with a gain of 158.7.

### **3.4.3 Controller**

All of the sensors and outputs of the system stemmed from the brain of the system, the DAQ controller. The first DAQ used to control the system was a NI DAQPad-6052E, which is an older piece of data acquisition hardware, and caused some issues with the new software used to control the system. The DAQpad-6052E connected easily through firewire to a computer and has BNC connectors to attach up to nine inputs and two outputs. Although the DAQPad-6052E could have been suitable for this project, the software interfacing issues eventually slowed the project down too much and forced the change to a new DAQ controller.

The DAQ controller used in the final system was the NI USB-6215 data acquisition system, which easily connects to a computer via a USB interface and comes with seven analog inputs and two analog outputs, which was more than enough for the two input signals and one output signal necessary for the wing test set-up. The controller was set-up to receive voltage input signals representing the position of the linear actuator and the force output of the actuator. The voltage output of the DAQ controller was used to send the driving signal to the actuator. After all of the wiring was hooked up and the DAQ

controller is connected to the computer, the software can control the wing and tests can be performed.

### **3.5 *Driving Software and PID Control***

One of the most difficult aspects of building this system was programming the software in Labview to flap the wing and run the tests. The process of writing the program can be broken down into a series of steps:

1. Read inputs clearly
2. Deliver reliable outputs
3. Maintain a constant position of the linear actuator (using a steady voltage output)
4. Gain position control with a varying input such as a sine wave
5. Write the data to a file

These tasks are all relatively simple individually, but when combined to make a unified system, they can be rather difficult to debug.

The software for the system was written using LabView, a program created by National Instruments that can be used to control the DAQ devices such as the USB-6215. LabView uses a graphical programming language that allows all of the code to be created by simply adding and connecting different blocks to create a virtual instrument (vi). Some of the blocks are complex and are classified as sub-vis and can perform sophisticated actions such as PID control. The software for this system was designed largely using the aid of online examples and videos from the Developer Zone of the National Instruments

website ([www.zone.ni.com](http://www.zone.ni.com)). These examples gave sample code for all of the different subcomponents of the problem, reducing the problem to simply connecting the different parts together.

The actual code for a LabView virtual instrument file is broken up into two sections, a front panel and a block diagram. The front panel contains all of the controls and graphs and is used to control the experiment, change parameters, and monitor the inputs and outputs of the system. The block diagram is essentially the inner workings of the system, it is where the program is actually designed and it shows all of the interconnections between the working components of the system. The block diagram is the place where the sub-vis mentioned earlier are used.

This section will explain the overview of all of the different components of the software, focusing on the back-end side of the program, the block diagram.

The block diagram of the final virtual instrument file is shown in Figure 24.

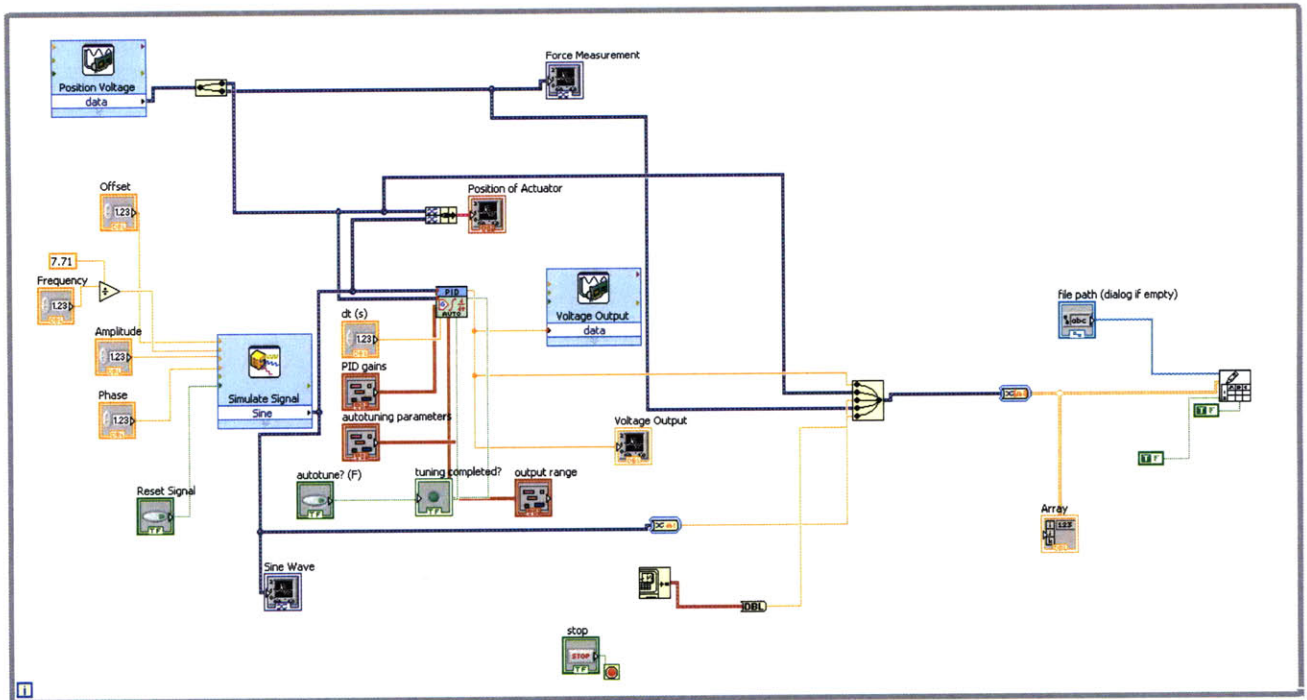


Figure 24: Block diagram of Labview virtual instrument.

The block diagram can be broken down into sections based upon the five primary tasks listed above. Each task will be analyzed along with a more detailed view of each appropriate section of the block diagram.

### 3.5.1 Read Inputs clearly

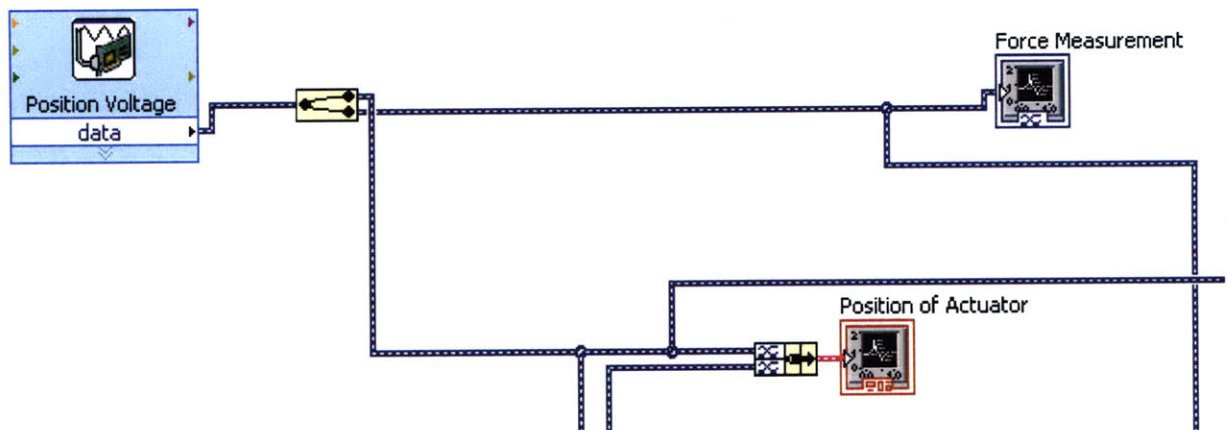
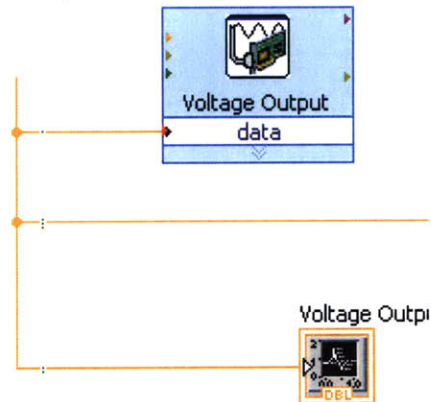


Figure 25: Block diagram of input section of Labview vi.

In order to read the analog inputs coming from the DAQ controller, a sub vi called the “DAQ assistant” can be used for the newer DAQ controllers. This capability was the main reason that the DAQ controller was switched from the original DAQPad-6052E to the newer DAQ USB-6215.

The DAQ assistant virtual instrument, in this case labeled “Position Voltage” pulls the input signals from the DAQ controller. Only one input DAQ assistant can be used per LabView file, requiring that all of the input signals come from the same sub-vi. In this case both the position measurement and the force measurement voltages are acquired by the “Position Voltage” vi. These signals are not useful when they are combined into one string of data, therefore they needed to be separated into individual signals before being displayed on the charts. The chart blocks are used to display any input data on the front panel so that the system can be monitored while it is running. In this case, the force measurement is sent directly to a chart to be displayed by itself, as it is not pertinent to compare the force to any other measure while you are running the system. Conversely, the input signal corresponding to the position of the actuator needs to be compared to the set point signal; therefore it is sent to a coupling block before going into the chart to be displayed.

### 3.5.2 Deliver Reliable Outputs



**Figure 26: Block diagram of output section of Labview vi.**

Like the task of acquiring the input signals, generating output signals made it necessary to upgrade to the USB-6215 as the output sub-vi is also the DAQ Assistant, this time named “Voltage Output”. This sub-vi works in a similar way to the input version of the DAQ Assistant except the main difference that it requires an input signal of some sort to know what voltage to output. Although this set-up seem relatively simple, the DAQ Assistant “Voltage Output” sub-vi is a rather complex block and performs many operations at once and must be tuned correctly in order to produce a reliable output.

### 3.5.3 Maintain Constant Position of the Linear Actuator (PID Control)

One of the most complex components of designing the software to operate the wing-actuator system was gaining discrete position control. This basically means the ability for the actuator to move to a specified position. In order to do this, a proportional-integral-derivative (PID) controller was used as the control scheme for the system.

A PID controller is a closed feedback loop that is widely used to control process parameters using relatively simple control methods. The integration of a PID controller is shown in Figure 27 below, with the following parallels to the actuator-wing system:

- Controller block  $C(s)$  represents the PID controller
- Process block  $P(s)$  represents the actuator-wing system
- Variable  $r$  represents the input set point for the system
- Variable  $y$  represents the actual position of the actuator
- Variable  $u$  represents the output voltage to the actuator

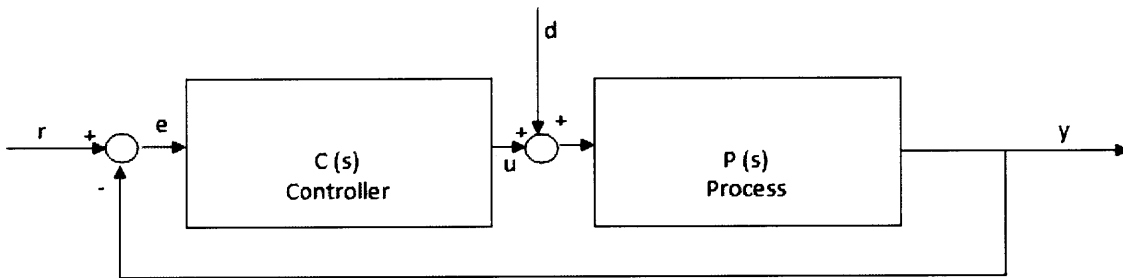


**Figure 27: PID control scheme.**

To control this system, each one of the PID elements contributes a different effect to ensure that the system is appropriately controlled.

- The proportional element or P represents the instantaneous difference between the actual position of the actuator and the desired input

- The integral element or I represents the integral of the past error of the system and uses the past error to keep the system stable
- The derivative element or D detects the instantaneous change in error in order to make an attempt to predict the future error

Each one of these elements needs to be tuned correctly in order to control the system properly. This can be a delicate process as incorrect parameters can cause the system to go unstable or to oscillate at an extremely high frequency and potentially cause damage to the system.

Tuning a PID controller is a widely studied topic and there are many methods available that can be used to find the proper values for the P, I and D elements. These methods often involve giving the system a steady voltage and adjusting the P value then inputting a sinusoidal curve and adjusting the I and D parameters appropriately. National Instruments also includes an auto-tuning PID controller sub-vi that can be used to automatically find the parameters and control the system simultaneously. Unfortunately this method has some drawbacks as it runs through a set program to find the parameters and sometimes sends the system into high amplitude and frequency oscillations that can damage the system without close operator supervision. Several attempts were made to auto-tune the actuator-wing system using the Labview sub-vi, but every attempt resulted in incorrect P, I and D parameters that sent the system out of control.

Ultimately the system was tuned manually using the knowledge of the effects of each of the tuning parameters. In order to tune it manually, the system was given a sine wave and the P value was determined first, then the I and D values were adjusted until a

reasonable control scheme was created. The final values for the parameters were  $P=0.5$ ,  $I=0.01$ , and  $D=0.001$ .

The actual PID controller itself is a sub-vi that can be installed into LabView with the PID control toolkit, which can be downloaded off of National Instruments website. Just like in the theoretical model, the PID controller needs inputs for the set-point, the present value, and the PID parameters. The output of the PID controller is an output value that corresponds with the driving voltage to the actuator. Figure 28 shows how the PID block can be wired into the system.

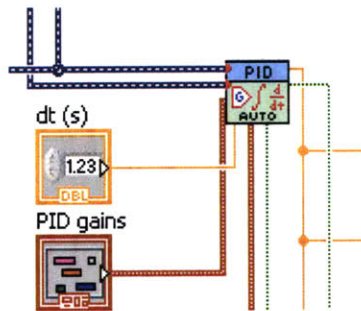


**Figure 28: Block diagram of PID section of Labview vi.**

### 3.5.4 Send a sinusoidal signal so that the wing can “flap”

Once position control was accomplished using the PID controller, the system was given a more interesting input. Making the wing “flap” required some sort of oscillating input. To keep things relatively simple a straight forward sine wave was selected as the input form. The sine wave will not perfectly imitate the motion of a flapping wing, but it will approximate it close enough to be able to characterize the actuator-wing system.

In order to create this sine wave, a sub-vi called “Simulate Signal” was used as shown in Figure 29. This block outputs a virtual signal based upon a number of inputs and controls

that change the output signal. The Simulate Signal sub-vi has options to output a constant signal, a sine wave, a triangle wave, or a square wave, for the reasons mentioned above a sine wave was used to stimulate the system.

The rest of the inputs into the Simulate Signal sub-vi are simple controls that affect the output such as the frequency of the sine wave, the offset, amplitude and phase. An issue arose with the frequency control, as the system moved at a frequency much higher than the input value. In order to adjust for this, the frequency was set to 1 Hz and the actual frequency of the system was measured. This data was then used to find that the system was moving at a frequency 7.71 times the input value. In order to correct this discrepancy the input frequency was divided by 7.71 before being sent to the Simulate Signal sub-vi.

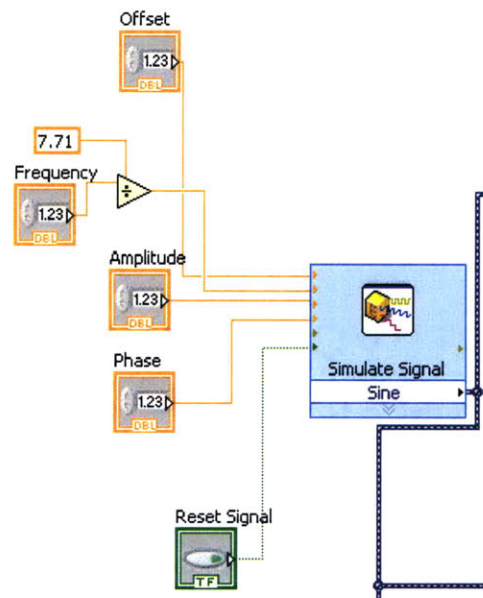


**Figure 29: Block diagram of signal simulator section of Labview vi.**

The output from the Simulate Signal sub-vi is then sent to the PID controller as the set-point, creating a sinusoidally changing set point that in turn drives the system in a sinusoidal manner.

### **3.5.5 Write the Data to a File**

The final step in the software file is writing all of the gathered data to a file. This component of the program was deceptively challenging due to the different types of signals that needed to be analyzed. Writing the data to a file required some creativity in order to get all of the signals to align so that they could be analyzed side by side in a useful manner. The five signals that needed to be recorded are shown below:

- Actual Position of the Actuator
- Desired position of the actuator (set point)
- Voltage from the force reading
- Output voltage that drives the actuator
- Time stamp

In order to write all of these signals to a file they were reduced to acceptable data formats, combined and written to a spreadsheet as shown below in Figure 30.

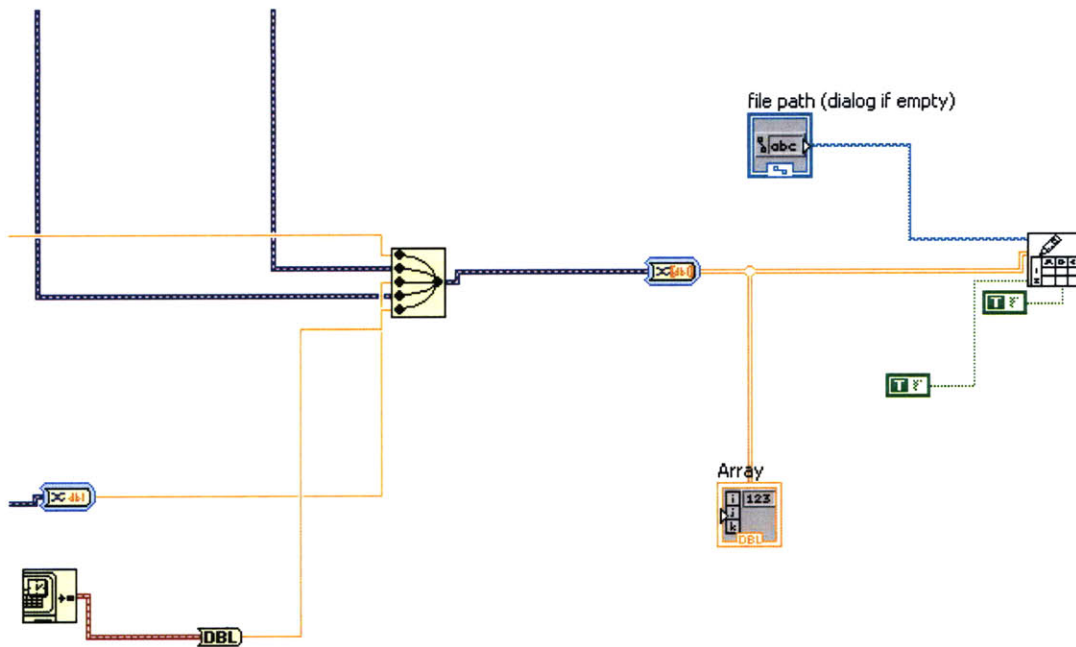


**Figure 30: Block diagram of file writing section of Labview vi.**

One of the main difficulties in reducing the data to acceptable forms was the varying sampling rates of the different signals. For instance, the simulated signal sampled 3000 times faster than the inputs or output could read or write. In order to solve this problem, the first number in each sampling period of 3000 was selected so that the sampling rate would match up with the other signals. A time stamp was created to ensure that all of the signals could be easily compared to each other and that the signals could be related to known amount of time. The time stamp function gives a value of the number of seconds since December 10<sup>th</sup> 1903 – resulting in a very large number, this is not a serious issue as the first number in each data set can be subtracted from each subsequent time value once the data is written into the spreadsheet, giving a relative time scale.

Once the data has been reduced and a time scale has been created, all of the signals can be merged together and written to a file. The “Write to Spreadsheet” sub-vi takes each set of five values and writes them to a file. This entire operation is put into a “while” loop so that it repeats itself, and the Write to Spreadsheet sub-vi simply appends the new sets of five points onto the end of the data file, giving a large set of data to work with in an excel spreadsheet format that can easily be analyzed.

## **4. Results and Discussion**

Once the entire system was built and set-up, the wing-actuator system could be tested to determine the effect of the important parameters on the performance of the actuator.

### **4.1 Testing the Wing**

The purpose of the building the test set-up with the wing and the power control system was to test the performance characteristics of the linear actuator using a real physical system. In order to test the wing actuator set-up, three variables were altered in order to see the effect of changing the set-up of the system.

1. Mounting Position of Wing Connector
2. Frequency of Oscillation
3. Sweep amplitude

The first variable that was changed was the mounting position of the wing connector. The idea behind this parameter is to see the effect of having the wing's neutral point be higher or lower in the actuator. This parameter was varied at three different values. The first position was one where the level point of the wing was higher up on the actuator which meant that the sweep angle never went very high at the top of the stroke. Another mounting position was chosen so that the level point of the wing was very low on the actuator, creating very shallow sweep angles at the bottom of the strokes. The final position was in the middle, leaving room for moderate sweep angles at the top and bottom of the stroke. Figure 31 shows the comparisons between the different mounting positions.

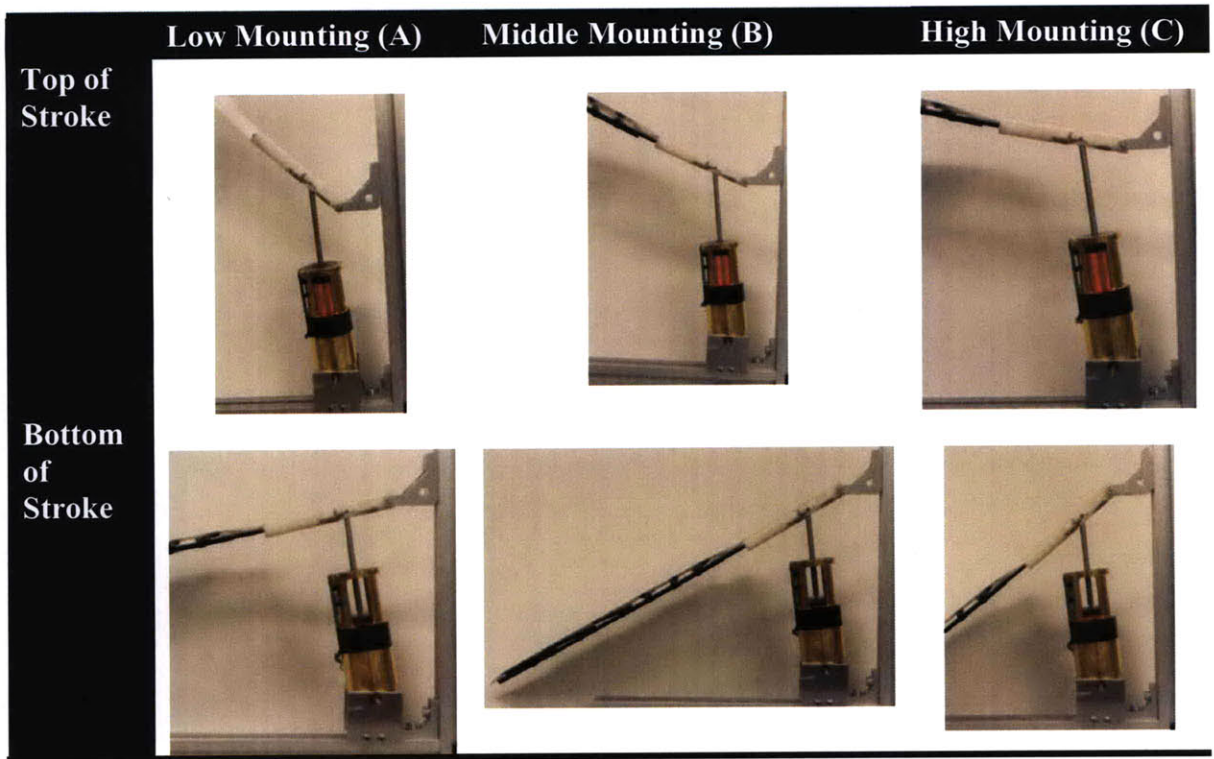


**Figure 31: Comparison of mounting positions for wing point.**

The next parameter that was changed during the testing of the wing was the oscillation frequency. Testing oscillation frequencies is important because FWF flight requires a wide range of frequencies to be able to perform all of the maneuvers; therefore the actuator should be able to handle a wide range of frequencies. The range of frequencies tested was in between 0.1 and 5 Hz. This is comparable to the natural oscillation frequencies of birds.

The final parameter that was tested was the sweep amplitude of the wing. In many of the reports the sweep amplitude was defined as the angle that the wing moves through in a stroke. For the purpose of this experiment, the sweep amplitude was approximated as the position of the actuator. Defining the sweep amplitude as this value will allow the effects

of the mounting position and the position of the actuator to be analyzed separately. Sweep amplitudes were varied between 10 and 100% of the range of the actuator.

In order to test each of these variables, the system was given a signal through the LabView program and a unique data file was written for each set of conditions. This combination of changing parameters resulted in 90 data files being written and analyzed.

## **4.2 Results and Significance**

After all 90 tests were run, the data was analyzed to see the effects of the different variables on the performance of the wing-actuator system.

All of the data was captured in voltages and therefore it needed to be converted to usable information before being analyzed. In order to do this, the sensors were all calibrated. As mentioned previously, the position sensor was calibrated by setting the actuator at different positions and recording the corresponding voltage. These measurements were correlated as shown in Figure 32. The resulting calibration curve gave a relationship of  $\text{Position} = -6.7476 \times \text{voltage} + 31.745$ . The  $R^2$  value of the calibration is very good at 0.9998.

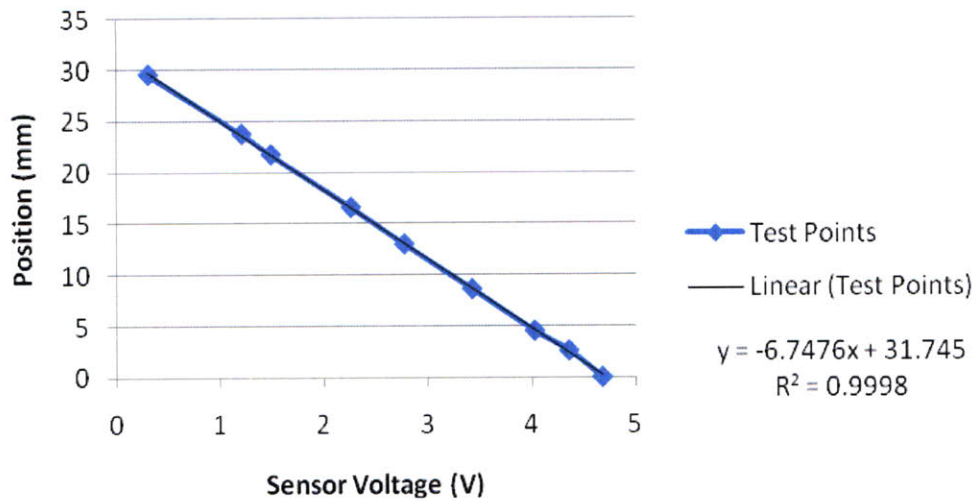


**Figure 32: Calibration curve for position sensor.**

The force measuring sensor also had to be calibrated, but required slightly more complex steps to ensure that the calibration was robust. The force sensor was calibrated by setting a stop for the actuator at different positions and then sending different output voltages to the actuator and measuring the force of the actuator using a handheld force sensor, which could then be related to the output voltage of the force measuring circuit. The stop was set at different positions to ensure that the position of the actuator did not significantly affect the force-voltage output relationship. Figure 33 shows the results of the calibration tests. Each set of points represents a different stop point for the actuator and the trend line is based off of an intermediate position of the actuator. The calibration relationship is  $\text{Force} = 3.2558 \times \text{output voltage} - 0.165$  with a strong  $R^2$  value of .9986. The only variation in the calibration comes when the actuator is almost fully extended, this information was taken into account when interpreting the final data.

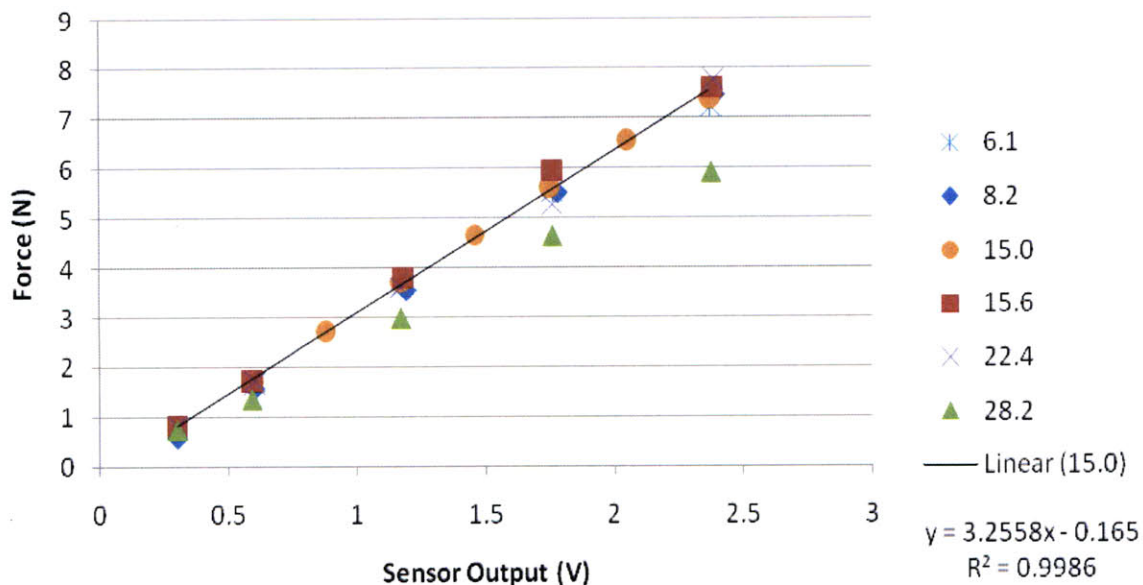


**Figure 33: Calibration curve for force sensor.**

The test produced force-position curves that look like ovals when a system is run periodically. The first trend that becomes obvious is that as the sweep amplitude decreased, the force on the motor is decreased. Figure 34 shows the effect of decreasing the sweep amplitude while keeping the mounting position and the oscillation frequency constant.

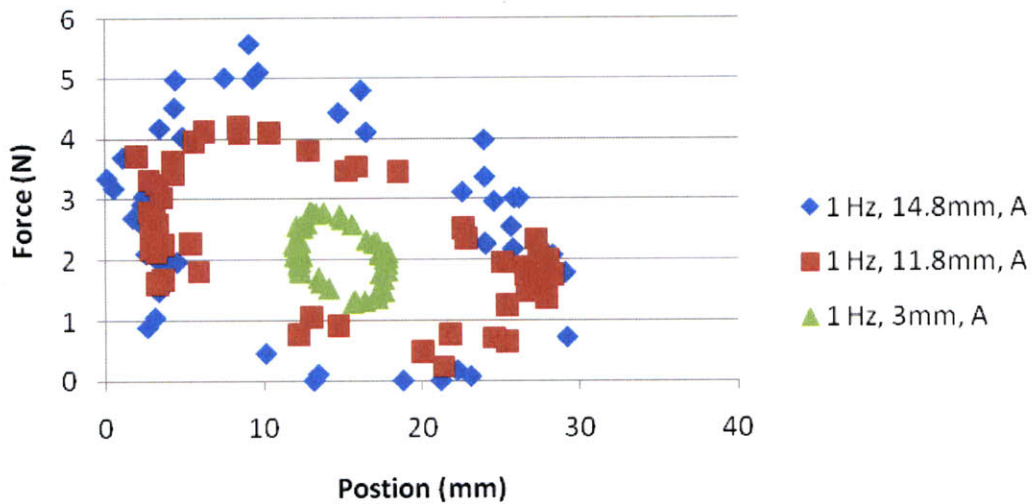


**Figure 34: Effect of sweep amplitude of actuator performance.**

As the sweep amplitude decreases, the force on the actuator decreases as well.

The next important relationship is how a change in oscillation frequency affects the force on the actuator. Figure 35 shows the force-position curves for several different frequencies with a constant mounting position and sweep amplitude. The relationship shows that as frequency increases, the force on the actuator increases.

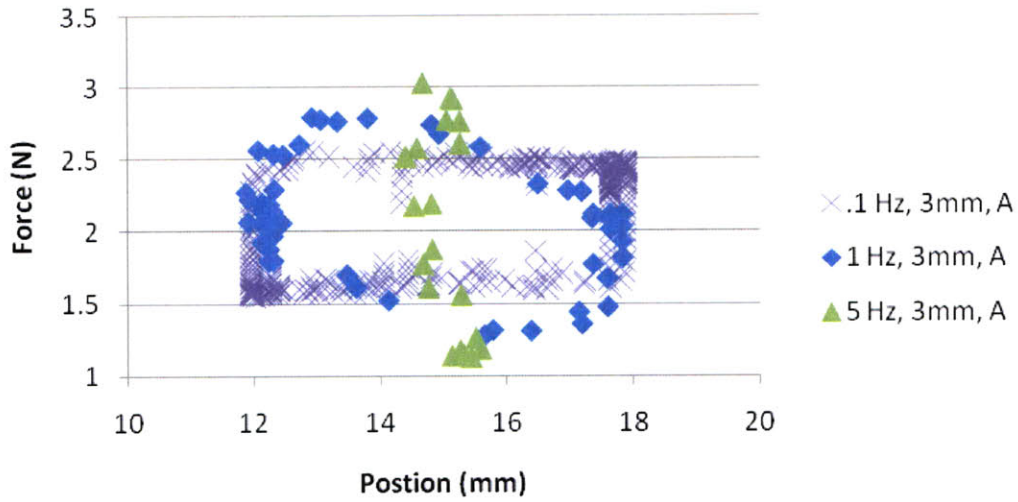


**Figure 35: Effect of oscillation frequency on actuator performance.**

It is important to note the difference in the data from the 5 Hz sample. When the system was run at a 5 Hz frequency the controller had troubles keeping up and therefore ended up oscillating at a lower sweep amplitude. Figure 36 shows the comparison between the desired position and the actual position of the actuator at 5 Hz.

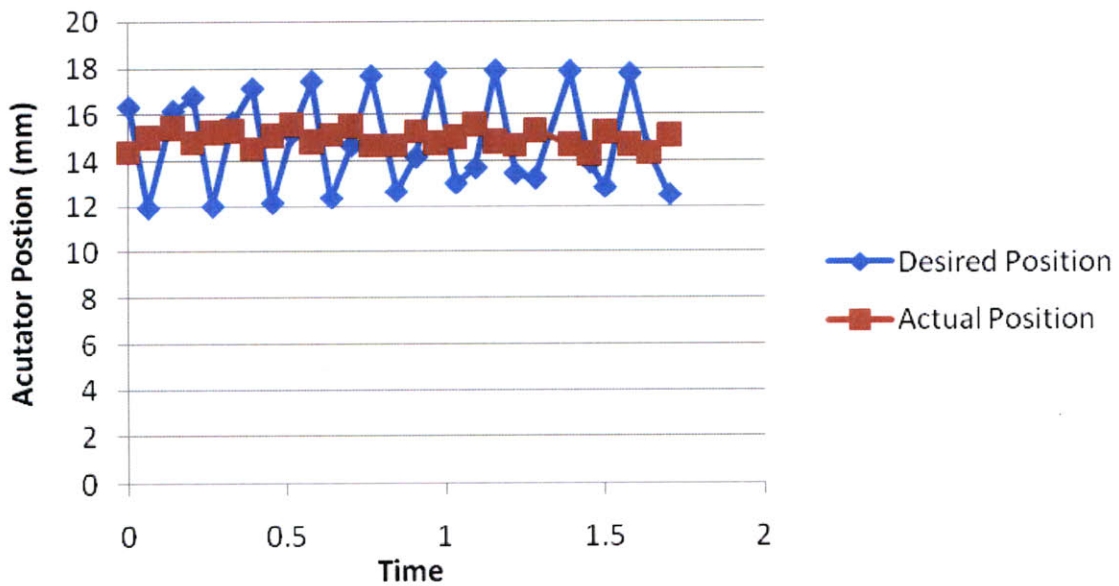


**Figure 36: Desired and actual position of actuator at 5 Hz.**

It is evident that the system controller cannot keep up with the demands of the input, causing the nearly flat position reading. This error can be attributed to the controller and not the actuator because the actuator is able to oscillate at 5Hz with a larger sweep amplitude if the input amplitude is increased.

The final parameter that was tested was the mounting position of the pivoting section of the wing. Figure 37 shows the data from three tests where the mounting position was changed and the frequency and amplitude were kept constant. It looks as though the mounting position of the wing is not an important parameter in the force output of the actuator as all three sets of data are similar to each other.

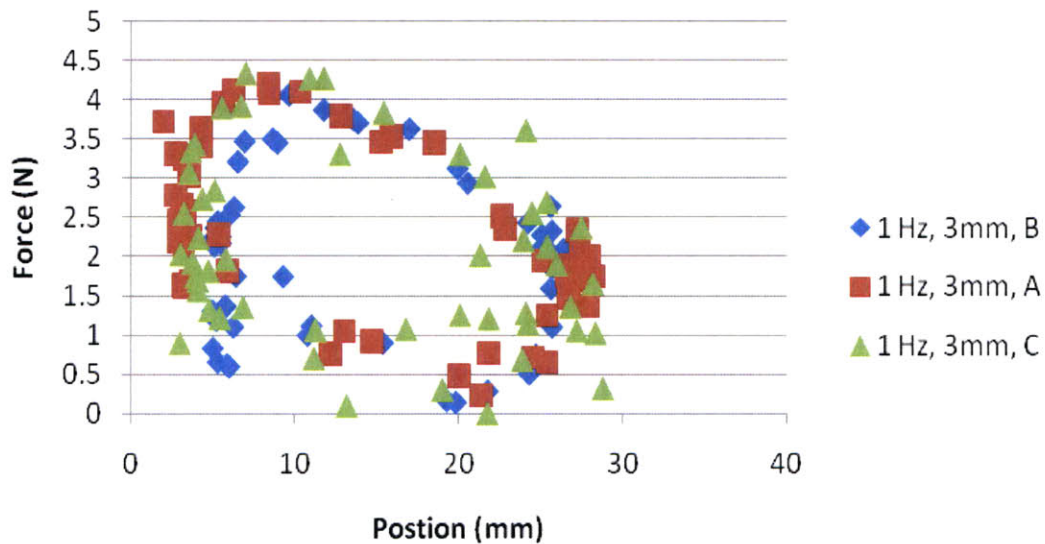


**Figure 37: Effect of wing pivot position on actuator performance.**

## 5. Conclusions and Future Work

The results of the testing show three important relationships in using this actuator attached to a wing.

1. An increase in sweep angle increases the force on the actuator,
2. An increase in frequency increases the force on the actuator,
3. There is no relationship between the mounting position of the pivot of the wing and the force output on the actuator.

The motion controller in this experiment was a limiting factor in collecting relevant information at higher frequencies. In future experiments, a more robust motion controller should be used to control the wing-actuator system. This will most likely take the form of a more refined PID system with more appropriate variables for the particular system. In order to do this a more robust auto-tuning software package may have to be used, as the ones built into Labview currently did not work with the system.

Throughout all of the tests, the actuator never seemed to have an issue reacting to the inputs it was given, even under high forces. In the future it may make sense to test the upper limits of the actuator as the voltage output of the power amplifier was set to 12.5 V, but the actuator could most likely handle a higher voltage, this limit would be useful to know before implementing it into a FWF UAV.

Another variable that could be tested is the attack angle of the wing. This is a more advanced parameter to characterize, but it is a critical parameter in FWF. In order to do

this – a similar battery of tests could be run while varying the attack angle along with the other three variables as well.

Another option for future study would be to modify the test rig to measure not only the net force on the actuator, but the lift and thrust forces as well by using horizontally and vertically aligned force sensors such as the set-up depicted in Figure 38<sup>6</sup>.

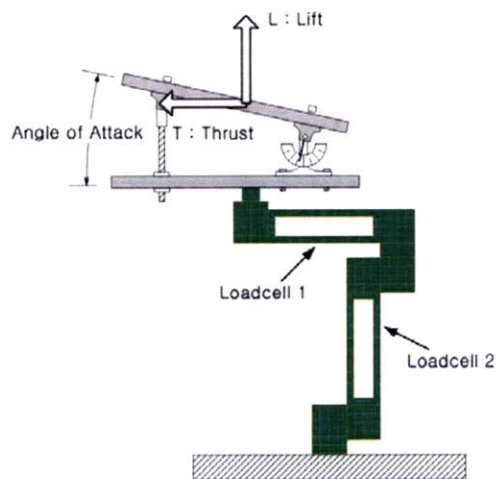


**Figure 38: Test set up including horizontal and vertical force sensors. Taken from Kim and Han.<sup>6</sup>**

## References

- 1 Araki, M. "PID Control." *CONTROL SYSTEMS, ROBOTICS, AND AUTOMATION* (1991). Web.
- 2 Ball, N. B. "An Optimized Linear Lorentz-Force Actuator for Biorobotics and Needle-Free Injection." Thesis. Massachusetts Institute of Technology, 2007. Print.
- 3 Dial, K. P., B. E. Jackson, and P. Segre. "A Fundamental Avian Wing-Stroke Provides a New Perspective on the Evolution of Flight." *Nature* (2008). Web.
- 4 Grand, Ch., P. Martinelli, J.-B. Mouret, and S. Doncieux. "Flapping-Wing Mechanism for a Bird-Sized UAVs: Design, Modeling and Control." *Advanced Robot Kinematics* (2008). Web.
- 5 Greenewalt, C. H. "The Wings of Insects and Birds as Mechanical Oscillators." *Proceedings of the American Philosophical Society* 104.6 (1960): 605-11. Web.
- 6 Kim, D., and J. Han. "Smart Flapping Wing Using Macro-Fiber Composite Actuators." *Smart Structures and Materials* (2006). Web.
- 7 Margerie, E. De, J. B. Mouret, S. Donciex, and J-A Meyer. "Artificial Evolution of the Morphology and Kinematics in a Flapping-wing Mini-UAV." *Bioinspiration and Biomimetics* (2007): 65-82. Web. 1 May 2010.
- 8 Pesavento, Umberto, and Z. J. Wang. "Flapping Wing Flight Can Save Aerodynamic Power Compared to Steady Flight." *Physical Review Letters* (2009). Web.
- 9 Poore, S. O., A. Ashcroft, A. Sanchez-Haiman, and G. E. Goslow. "The Contractile Properties of the M. Supracoracoideus in the Pigeon and Starling: A Case for Long-Axis Rotation of the Humerus." *Journal of Experimental Biology* (1997). Web.

- 10 Shang, J. K., S. A. Combes, B. M. Finio, and R. J. Wood. "Artificial Insect Wings of Diverse Morphology for Flapping-wing Micro Air Vehicles." *Bioinspiration and Biomimetics* (2009). Web.
- 11 Tobalske, B. W. "Biomechanics of Bird Flight." *Journal of Experimental Biology* (2007). Web.
- 12 "Wide Area Surveillance Projectile." *MIT*. Web. 07 Oct. 2009.  
<<http://web.mit.edu/aeroastro/www/labs/ICE/projects/wasp.html>>.

Hardman Adhesives, Milford, NH, <http://www.ellsworth.com/>

Kepeco Inc., Flushing, NY, <http://www.kepecopower.com/>

Loctite Corporation, Rocky Hill, CT, <http://www.loctite.com/>

MK Technology, Bloomfield, CT, <http://www.mknorthamerica.com/>

National Instruments, Austin, TX, <http://www.ni.com/>